RSC Advances

PAPER

View Article Online
View Journal | View Issue

Cite this: *RSC Adv.*, 2026, **16**, 29025

Antimicrobial efficacies and molecular 3D modeling of novel biopolymer derivatives extracted from biowaste using a solid-state mechanochemical technique

Murugaiyan Manimohan,*[a] Mohamed Aboobucker Sithique[a] and Sivashanmugam Pugalmani[b]

The biomass source, lobster shell waste, was converted into a useful biopolymer by acid–base treatment through a solid-state mechanochemical technique using ball milling. Cobalt(II), copper(II), and zinc(II) metal ion-inserted, novel biologically active, water-soluble nitrogen–nitrogen–oxygen (N,N,O) polydentate donor hydrazide-grafted *O*-carboxymethyl chitosan (*O*-CMCS) Schiff base metal complexes were prepared. Computational studies, including 3D molecular modeling and selected bond lengths and bond angles of metal complexes, were carried out using the PerkinElmer ChemDraw Professional 16.0 software. The complex formation between the novel Schiff base ligands and metal ions dramatically changed the bond angles and bond lengths of the Schiff base ligand due to the lone pair-lone pair repulsion in the active molecules. Fourier-transform infrared (FT-IR) and ultraviolet (UV)-visible spectral analyses confirmed the formation of metal complexes through the metal–oxygen (M–O) and metal-nitrogen (M–N) bonds. Scanning electron microscopy (SEM) and transmission electron microscopy (TEM) were employed to investigate the surface and internal morphological characteristics of the metal complexes. The bactericidal actions of the compounds were evaluated against *Escherichia coli*, *Staphylococcus aureus*, *Pseudomonas aeruginosa*, and *Bacillus subtilis* using a nutrient agar medium by the agar well-diffusion method. In addition, the *O*-CMCS Schiff base derivatives were tested against a few fungi. *Candida albicans* and *Aspergillus niger* showed higher percentages of growth inhibition, and the Zn(II) metal complexes exhibited better antifungal efficacy than the Co(II) and Cu(II) metal complexes.

Received 22nd January 2026
Accepted 11th May 2026

DOI: 10.1039/d6ra00600k

rsc.li/rsc-advances

1 Introduction

Seafood industries annually expel 6–8 million tons of arthropod waste, such as lobster, shrimp, and crab shells and other crustacean by-products. Roughly 40–50% of the lobsters are disposed of as biowaste, including their shells, heads, and other inedible parts. A lobster shell comprises 36% minerals, 29% proteins, and 25% chitin derivatives.[1] To reduce this biowaste, the hard exoskeletons, segmented bodies, and jointed appendages of arthropods can be treated through deproteinization and demineralization processes to produce chitin (CN). Chitin, a valuable by-product of lobster shells, is widely employed in various industries. It is a natural linear biopolymer comprising an amide group at the C_2 position of the pyranose ring.[2]

The conjugation of CN with other biopolymers enhances its pharmaceutical, biomedical and clinical applications, including the antibacterial and antifungal applications. Chitosan (CS) is prepared from CN through the deacetylation process.[3] In the past decade, many researchers have reported that chitosan and its derivatives act vigorously against pathogens due to the positive NH_3^+ ion in acidic media. In general, pathogens containing a negative cell membrane easily interact with the positive ions of chitosan, which neutralize the pathogenic activity.[4–6]

Biopolymer Schiff base ligands and their metal complexes have potential antimicrobial applications.[7–12] *O*-CMCS-cationic fungal membranes coated with liposome have shown enhanced antifungal effects.[13] Several studies have been reported on synthesizing chitosan Schiff base metal complexes due to their interesting and versatile applications, including their anticancer and antimicrobial efficacies.[14,15] Often, *O*-CMCS metal complexes are formed from a mixture of chitosan, a hydrazide-based precursor, and monochloroacetic acid, offering advantages like biocompatibility, low cost, eco-friendliness, and water solubility.[16,17] We used a single-step

[a]*PG & Research Department of Chemistry, Islamiah College (Autonomous), Tirupattur District, Vaniyambadi-635752, Tamil Nadu, India. E-mail: manimohanchem@gmail.com; Tel: +91-8870617066*

[b]*Saveetha Institute of Medical and Technical Sciences, Chennai-600077, Tamil Nadu, India*

green synthesis to extract low molecular weight chitin (LMw-C) with a molecular weight of less than 100 kDa from lobster shell waste by demineralization and deproteinization under mild acid–base conditions using a solid-state mechanochemical technique.[18]

We obtained LMw-C with 80–90% purity and a molecular weight of 85 kDa molecular weight under 5 wt% acid conditions at 100 °C for 10 h.[19] As in Manimohan *et al.*, this research work is pioneering towards the treatment of secondary lymphedema, which may potentially be cured using low-molecular-weight polymers that enhance lymphatic drainage and reduce the fibrotic nature of the lymphatic vessel.[20] Production of lobster shell waste results in huge waste deposits. To reduce this waste and develop economic management strategies, we prepared a valuable product, chitin, from waste heaps through a green approach. To the best of our knowledge, no remarkable research has been reported on novel water-soluble hydrazide coordinated chitosan Schiff base metal complexes synthesised through the solid-state mechano-chemical technique using a ball mill.

2 Experimental section

2.1 Materials and methods

Lobster (*Panulirus argus*) shell waste was collected from Supreme Seafood, Patinapakkam, Chennai. Cobalt(II) acetate, copper(II) acetate, zinc(II) acetate, sodium hydroxide, dimethyl formamide (DMF), acetone, toluene, and dimethyl sulphoxide (DMSO) were purchased from Sigma-Aldrich, Avra, and SRL India. Bacterial strains such as *Escherichia coli* (CAS No. 68583-22-2), *Staphylococcus aureus* (68583-38-0), *Pseudomonas aeruginosa* (CAS No. 68583-29-9) and *Bacillus subtilis* (CAS No. 68038-70-0), as well as fungal strains such as *Aspergillus niger* (CAS No. 9001-05-2), and *Aspergillus clavatus* (CAS No. 36011-19-5) were selected due to their pharmaceutical and clinical importance. All chemicals used in this study were of analytical reagent (AR) grade.

2.2 Analytical methods

Chitin powder was prepared using a Fritsch P-5 High Energy Planetary Ball Mill-3 operating with an extra-strong 2.2 kW drive power, producing centrifugal acceleration up to 64 g and rotational speeds up to 800 rpm, with a bowl rotational speed of 1600 rpm. The FT-IR spectra were recorded using a PerkinElmer Spectrum Version 10.4.00 spectrometer in the operating range of 4000–400 cm^{-1} using the KBr pellet method. The confocal micro-Raman spectrometer recorded the metal complexes at 532 nm using the laser source. The X-ray diffraction (XRD) patterns were recorded using a Bruker D8 Advance diffractometer (Germany) equipped with Cu Kα radiation ($\lambda = 0.15406$ nm). The instrument was operated at an applied voltage of 40 kV and a current of 30 mA. The diffraction patterns were recorded with the scan rate of $2\theta = 0.02°$ and angle range from 10° to 90°. The morphological surface and internal structure of the metal complexes were investigated using a scanning electron microscope (SEM) and high-resolution transmission electron microscope (HRTEM) with a 200 kV accelerating voltage (JEOL JEM 2100 model). The energy dispersive X-ray analysis (EDAX) spectra of the metal complexes were recorded using an electron microscope (Thermo Fisher Scientific, FEI Company, USA). A viscometry study was carried out to determine the viscosity-average molecular weight (M_v) of the chitosan using the Mark–Houwink equation, $[\eta] = K(M_v)\ \alpha$. The carbon (^{13}C) and proton (^{1}H) nuclear magnetic resonance (NMR) spectra were recorded using a 400 MHz Bruker NMR spectrometer, with heavy water (D_2O) used as the solvent.

2.3 Antimicrobial efficacies

The antibacterial activities of the biopolymer Schiff base and the derivatives were evaluated using the agar plate method. Nutrient agar and potato dextrose agar media (Microcare Laboratory, Surat, India) were used for maintaining the bacterial stock cultures. The stock cultures were incubated at 37 °C for 24 h and subsequently stored at 4 °C in a refrigerator. Then, the bacterial strains were cultured on Mueller–Hinton agar (MHA) plates and incubated at 37 °C. Yeasts and molds were grown on Sabouraud dextrose agar (SDA) and potato dextrose agar (PDA) media, respectively, at 27 °C. The polymer Schiff base and its derivatives (10 mg/10 mL) were dissolved in water and DMSO, respectively. The percentage inhibition of bacterial growth was determined by measuring the diameter of the inhibition zones using an inhibition zone reader and was calculated using the following formula:

$$\text{Percentage inhibition of bacterial growth} = [(A_c - A_t)/A_c] \times 100, \quad (1)$$

where A_c and A_t are the inhibition zones of the test and control plates in diameter (mm), respectively. The antifungal activities of the biopolymer Schiff base and the metal complexes were studied against selected fungal pathogens using the agar diffusion method. Potato dextrose agar (PDA) medium was used for maintaining fungal cultures. The fungal stock culture was incubated for 24 h and then refrigerated at 4 °C. The microbiological growth medium Mueller–Hinton agar (MHA) was employed for antifungal testing and to grow various fungal strains at 37 °C. SDA and PDA media were employed to grow the yeasts and molds at 28 °C. The selected fungal stock cultures were maintained separately at 4 °C. The polymer metal complexes (10 mg/10 mL) were dissolved in DMSO, and ampicillin (10 mg/10 mL) was used as the reference drug. The prepared plates were incubated at 37 °C for 24 h. Statistical analysis was carried out using the zone inhibition method for the antimicrobial studies, and the level of significance was evaluated at $p < 0.05$. All experiments were performed in triplicate ($n = 3$). Data are expressed as mean ± standard deviation.

2.4 Extraction and preparation: deacetylated chitosan

The biopolymer chitosan was extracted from lobster shell waste through demineralization and deproteination under mild conditions using acid base treatment, and the water-soluble substituted biopolymer-embedded Schiff base ligands were

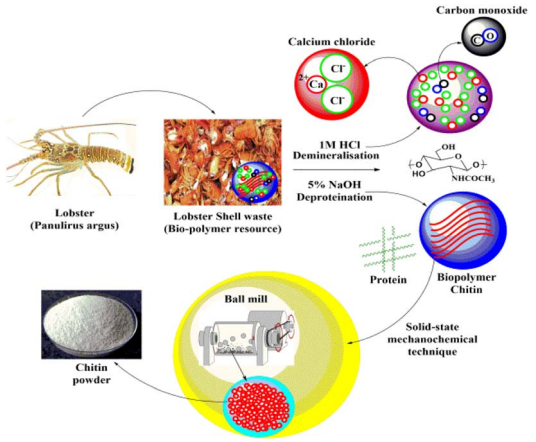

Scheme 1 Extraction and preparation of chitin from lobster (*Panulirus argus*) shell waste through a solid state mechano-chemical technique. Collected lobster shell waste was subjected to deproteination (5% NaOH) and demineralisation (1 M HCl) until the product became neutral through acid–base treatment. The figure shows that unwanted minerals, such as calcium chloride and carbon monoxide, were removed during the process. The eliminated protein was removed as flesh and scum, like fatty oil and calcium chloride, and gases, like carbon oxides, and other minerals were removed as white lime deposits. Afterwards, the dried product was ball-milled for solid-state mechano-chemical treatment and ground well to obtain the powdered biopolymer as shown in the figure.

prepared as reported in our previous studies.[20,21] The extracted lobster shell biowaste was washed thoroughly and dried at 65 °C to obtain stable chitosan powder. Afterward, the polymer was obtained without biowaste generation through a recently reported green approach, namely, the solid-state mechano-chemical treatment method, by mixing biopolymer and NaOH in a 1 : 5 (w/v) ratio. The mixture was then finely powdered using a ball mill for 30–90 minutes (Scheme 1). Afterwards, the resulting product was washed well several times with demineralized water until the amide moieties were removed from the polysaccharide chain of the polymer. The chitin powder was then dried at 50 °C in a hot air oven for 8 h. Finally, the obtained polymer was utilized for the synthesis of biopolymer Schiff base derivatives.[22,23]

2.5 Preparation of water-soluble biopolymer/hydrazide blended *O*-carboxymethyl chitosan Schiff base ligand through an *in situ* synthesis

The extracted chitosan possesses a low molecular weight of approximately 85 kilodaltons (kDa). The degree of deacetylation increased with an enhanced ratio of NaOH during the deacetylation of the chitin. The chitosan was deacetylated to about 80–90%, which was confirmed through potentiometric titration (Fig. S1). After complete deacetylation, the chitosan was dissolved in a weak acidic medium (acetic acid) and stirred well for 1 h in an oil bath. Subsequently, the Schiff base precursors IA, BHA, HBA, ID, BHD, and HBD were synthesised by reacting [1]β-diketones, namely, 3-methylpentane-2,4-dione and 2-methyl-1,3-diphenylpropane-1,3-dione (1 mol), along with substituted hydrazides (1 mol), such as 4-bromobenzohydrazide, isoniazid, and 4-aminobenzohydrazide, respectively, at 60 °C in a 1 : 1 molar ratio. In detail, the β-diketone and substituted benzohydrazide were dissolved in ethanol and concentrated at 45 °C until a yellow coloured solution was obtained. Then, the concentrated solution was added slowly into the deacetylated chitosan (3-fold of DCS) solution under continuous stirring using a magnetic stirrer in a silicone oil bath. Afterwards, 2.5 g of monochloroacetic acid in 10 mL of ethanol solution was added to the reaction mixture, and stirring was continued until a yellow-orange solid formed. The resulting yellow-orange solid was treated with hot ethanol and methanol to remove the unreacted substances and dried at 60 °C in a hot air oven for 4 h.

2.6 Synthesis of Co(II), Cu(II), and Zn(II) metal complexes of Schiff base ligands

0.3 g of substituted Schiff base ligands (IA-OCMCS, BHA-OCMCS, HBA-OCMCS, ID-OCMCS, BHD-OCMCS, and HBD-OCMCS) was dissolved separately in 20 mL of double-distilled water, then 20 mL of a water solution of $Co(CH_3COO)_2 \cdot 4H_2O$ (0.5 g) was added to each vessel.

Similarly, 0.3 g of Schiff base ligands was dissolved separately in 20 mL water, then 20 mL of a water solution of $Cu(CH_3COO)_2 \cdot H_2O$ (0.5 g) was added to each vessel, and 20 mL of Schiff base ligands (0.3 g) was dissolved separately in 20 mL of $Zn(CH_3COO)_2 \cdot 2H_2O$ (0.5 g) in each vessel. All the reaction mixtures were stirred at 600 rpm in an oil bath maintained at 50 °C for 8 h and then allowed to cool to room temperature, resulting in the formation of precipitates [OCMCS-$Co(OAc)_2$: pale pink, OCMCS-$Cu(OAc)_2$: green and OCMCS-$Zn(OAc)_2$: reddish brown]. Subsequently, the precipitates were washed several times with 2D (double distilled) water until pure metal complexes were obtained. Finally, the resulting polymeric compounds were dried in an air oven at 60 °C for 6 h (Scheme 2). The percentage yields (%) of the biopolymer Schiff bases and their Co(II), Cu(II), and Zn(II) complexes were calculated and are represented in Table S1.

3 Results and discussion

3.1 Solubility

The solubility of the prepared compounds was tested at room temperature using various solvents, including water, acetic acid (AcOH), methanol (MeOH), ethanol (EtOH), toluene, dimethylsulphoxide (DMSO), and dimethyl formamide (DMF). The solubility results of the prepared compounds are represented in Table S2.

3.2 Spectroscopic analysis

FT-IR spectroscopic analysis was employed to identify the various functional groups present in the polymer and its derivatives. An ICP-OES elemental analyser was used to determine the elemental composition of the prepared compounds. UV-visible spectral analysis was carried out to investigate the metal coordination with the Schiff base ligand. The bathochromic (red) shift observed in the complexes was confirmed

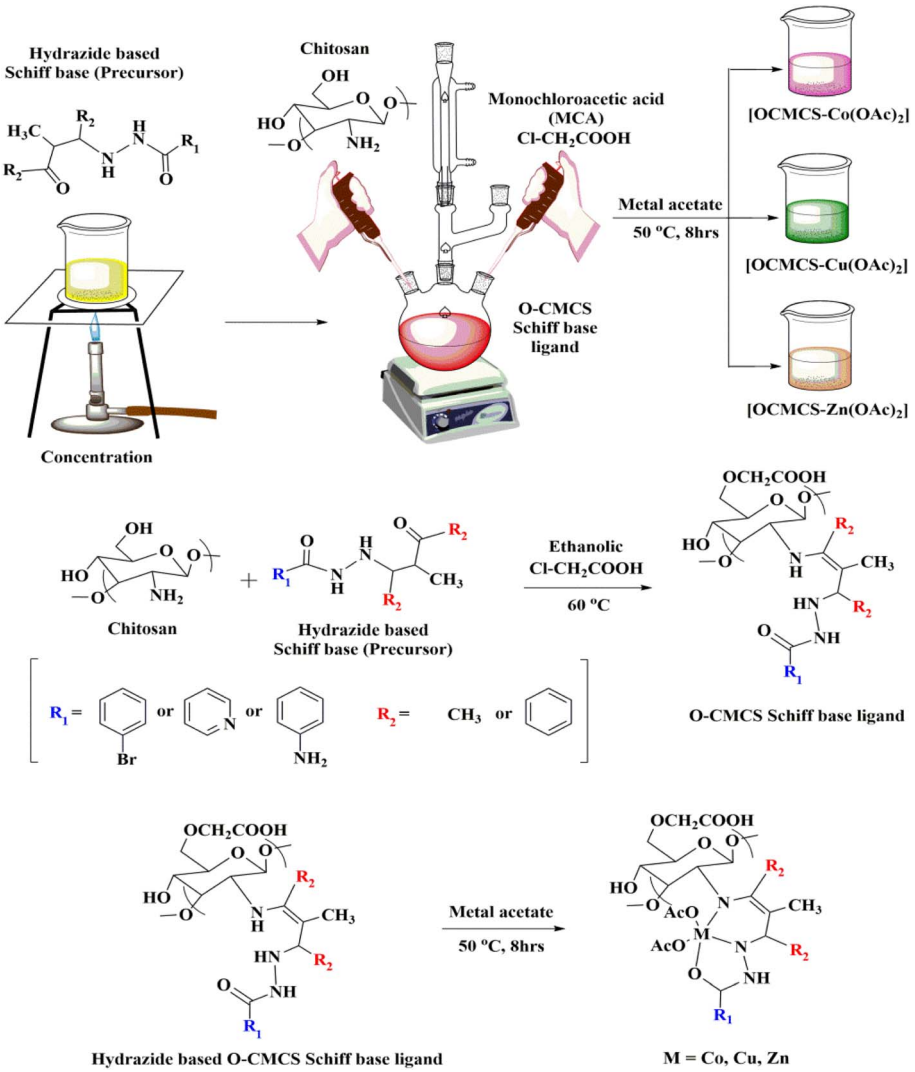

Scheme 2 Preparation of the precursors 4-bromo benzohydrazide (BHA)-, isoniazid (IA)-, and 4-amino benzohydrazide (HBA)-blended ^{1}β-diketone with 3-methylpentane-2,4-dione and 4-bromo benzohydrazide (BHD)-, isoniazid (ID)-, and 4-amino benzohydrazide (HBD)-blended ^{2}β-diketone with methyl-1,3-diphenylpropane-1,3-dione. The incorporation of the biopolymer Schiff base ligand (*O*-CMCS) to the prepared precursors (IA, BHA, HBA and ID, BHD, and HBD) leads to the formation of the Schiff base ligands, such as IA-OCMCS, BHA-OCMCS and HBA-OCMCS by the ^{1}β-diketone and ID-OCMCS, BHD-OCMCS and HBD-OCMCS by the ^{2}β-diketone. The formation of the pink Co(II) metal complexes, green Cu(II) metal complexes, and pale yellow Zn(II) metal complexes gives a total of eighteen metal complexes.

through the maximum range of absorption towards the visible region. Additionally, the SEM and X-ray diffraction studies confirm the interaction between the Schiff base compounds and the metal ions. Elemental analysis of the prepared metal complexes was carried out to determine the percentages of carbon, hydrogen, nitrogen, and metal ions found in the prepared compounds. The theoretical percentages of C, H, and N for the metal complexes were calculated using the ChemDraw Professional 16.0 software, and the calculated values were found to be in good agreement with the results of the elemental analysis.[24] After insertion of the metal ions, the C, H, and N content percentages in the *O*-CMCS derivatives decrease, confirming the formation of metal complexes. The elemental compositions (C, H, N, and metal ions) of the polymer compounds (in percentage) are as follows. IA-OCMCS: C-50.96, H-6.08, N-7.42; BHA-OCMCS: C-51.91, H-7.18, N-11.88; HBA-OCMCS: C-54.08, H-7.03, N-10.77; ID-OCMCS: C-60.71, H-5.48, N-6.11; BHD-OCMCS: C-62.76, H-6.61, N-9.54; HBD-OCMCS: C-63.86, H-6.48, N-9.61; [(IA-OCMCS)-Co(OAc)$_2$]: C-43.68, H-5.16, N-5.96; Co-11.46, C/N-7.32; [(BHA-OCMCS)-Co(OAc)$_2$]: C-45.13, H-5.77, N-8.78, Co-10.81, C/N-5.14; [(HBA-OCMCS)-Co(OAc)$_2$]: C-45.49, H-5.64, N-8.55, Co-11.17, C/N-5.32; [(ID-OCMCS)-Co(OAc)$_2$]: C-51.21, H-4.88, N-4.96, Co-14.87, C/N-10.32; [(BHD-OCMCS)-Co(OAc)$_2$]: C-53.73, H-5.78, N-7.26, Co-12.61, C/N-7.40 and [(HBD-OCMCS)-Co(OAc)$_2$]: C-54.93, H-5.24, N-7.12, Co-14.01, C/N-7.71.

Similarly, the C, H, and N elemental analysis and ICP-OES data for copper complexes (in %) are as follows: [(IA-OCMCS)-Cu(OAc)$_2$]: C-41.38, H-4.61, N-5.76, Cu-13.18, C/N-7.18; [(BHA-OCMCS)-Cu(OAc)$_2$]: C-46.68, H-5.73, N-8.71, Cu-16.18, C/N-5.36;

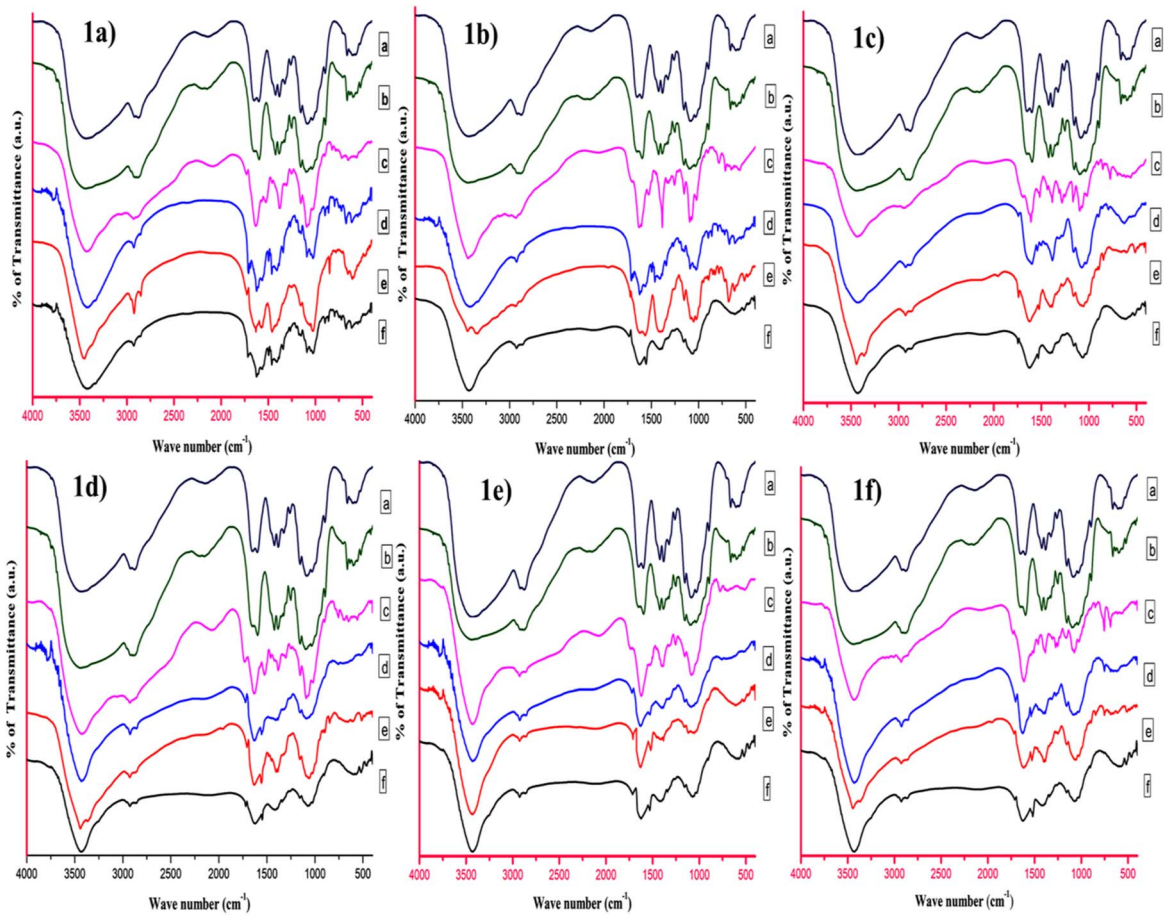

Fig. 1 Fourier transform infra-red spectra of the chitosan extracted from lobster shell waste, the prepared biopolymer Schiff bases and their Co(II), Cu(II) and Zn(II) metal complexes. The figures show the FT-IR spectra plotted between the transmission percentage and wavenumber in cm^{-1}. (a) FT-IR spectra of the (a) biopolymer (CS), (b) fully deacetylated (DCS), (c) Schiff base ligand (IA-OCMCS), and their metal (d) Co(II), (e) Cu(II), and (f) Zn(II) complexes. (b) FT-IR spectra of the (a) biopolymer (CS), (b) DCS, (c) Schiff base ligand (BHA-OCMCS), and their (d) Co(II), (e) Cu(II), and (f) Zn(II) metal complexes. (c) FT-IR spectra of the (a) biopolymer (CS), (b) DCS, (c) HBA-OCMCS, and their (d) Co(II), (e) Cu(II), and (f) Zn(II) metal complexes. (d) FT-IR spectra of the (a) CS, (b) DCS, (c) ID-OCMCS, and their (d) Co(II), (e) Cu(II), and (f) Zn(II) metal complexes. (e) FT-IR spectra of the (a) biopolymer (CS), (b) fully deacetylated (DCS), (c) BHD-OCMCS, and their (d) Co(II), (e) Cu(II), and (f) Zn(II) metal complexes. (f) FT-IR spectra of the (a) biopolymer (CS), (b) fully deacetylated (DCS), (c) HBD-OCMCS, and their (d) Co(II), (e) Cu(II), and (f) Zn(II) metal complexes.

[(HBA-OCMCS)-Cu$(OAc)_2$]: C-47.27, H-5.62, N-8.66, Cu-16.18, C/N-5.46; [(ID-OCMCS)-Cu$(OAc)_2$]: C-51.63, H-4.84, N-4.93, Cu-11.26, C/N-10.47; [(BHD-OCMCS)-Cu$(OAc)_2$]: C-52.92, H-5.47, N-7.19, Cu-14.32, C/N-7.36 and [(HBD-OCMCS)-Cu$(OAc)_2$]: C-53.19, H-5.39, N-7.13, Cu-12.88, C/N-7.46. Similarly, the elemental analysis and the ICP-OES data for the zinc complexes (in %) are as follows: [(IA-OCMCS)-Zn$(OAc)_2$]: C-43.18, H-4.88, N-5.86, Zn-9.18, C/N-7.37; [(BHA-OCMCS)-Zn$(OAc)_2$]: C-46.87, H-6.08, N-8.87, Zn-10.63, C/N-5.28; [(HBA-OCMCS)-Zn-$(OAc)_2$]: C-45.29, H-5.73, N-8.52, Zn-12.05, C/N-5.32; [(ID-OCMCS)-Zn$(OAc)_2$]: C-51.51, H-4.86, N-5.09, Zn-7.48, C/N-10.12; [(BHD-OCMCS)-Zn$(OAc)_2$]: C-52.04, H-5.63, N-7.27, Zn-9.13, C/N-7.16 and [(HBD-OCMCS)-Zn$(OAc)_2$]: C-52.07, H-5.45, N-7.11, Zn-11.02, C/N-7.32. The porosities (ϕ) of the polymer Schiff bases and their Co(II), Cu(II), and Zn(II) metal complexes were calculated in percentage using the following formula:

$$\text{Dry state porosity}(\phi) = \frac{(1 - V_{ma})}{V_b} \times 100, \quad (2)$$

where V_{ma} is the volume of the matrix and V_b is the bulk volume of the polymer derivatives.

The porosities (ϕ) of the prepared polymer derivatives[25] are as follows: [(IA-OCMCS)-Co$(OAc)_2$]: 5.12, [(BHA-OCMCS)-Co$(OAc)_2$]: 4.81, [(HBA-OCMCS)-Co$(OAc)_2$]: 3.12, [(ID-OCMCS)-Co$(OAc)_2$]: 4.86, [(BHD-OCMCS)-Co$(OAc)_2$]: 4.53, [(HBD-OCMCS)-Co$(OAc)_2$]: 5.84, [(IA-OCMCS)-Cu$(OAc)_2$]: 4.32, [(BHA-OCMCS)-Cu$(OAc)_2$]: 5.12, [(HBA-OCMCS)-Cu$(OAc)_2$]: 3.38, [(ID-OCMCS)-Cu$(OAc)_2$]: 4.36, [(BHD-OCMCS)-Cu$(OAc)_2$]: 2.78, [(HBD-OCMCS)-Cu$(OAc)_2$]: 4.48, [(IA-OCMCS)-Zn$(OAc)_2$]: 3.64, [(BHA-OCMCS)-Zn$(OAc)_2$]: 4.61, [(HBA-OCMCS)-Zn$(OAc)_2$]: 3.02, [(ID-OCMCS)-Zn$(OAc)_2$]: 2.94, [(BHD-OCMCS)-Zn$(OAc)_2$]: 3.63 and [(HBD-OCMCS)-Zn$(OAc)_2$]: 3.58.

The viscosity-average molecular weight (M_v) of the chitosan was determined using the Mark–Houwink equation, $[\eta] = K(M_v)\alpha$. Here, $[\eta]$ represents the intrinsic viscosity of chitosan after depolymerisation, while K and α are system-specific constants. The constants for the chitosan-solvent system were determined experimentally to be $K = 1.38 \times 10^{-5}$ and $\alpha = 0.86$. The

Table 1 XRD spectra and the assignments of 4-bromo benzohydrazide, isoniazid, and 4-amino benzohydrazide-based biopolymer *O*-carboxymethyl chitosan Schiff base ligand and its Co(II), Cu(II), and Zn(II) complexes

Sl. no.	Biopolymer and its derivative	XRD spectra	Assignment
1	Chitosan (CS)	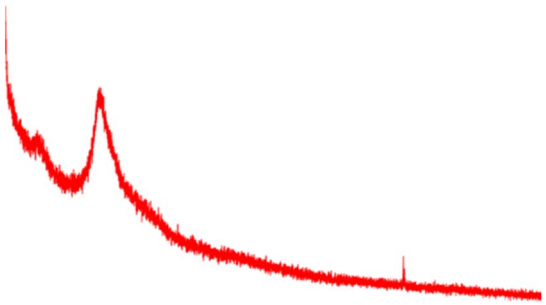	Responsible for the amide (–NH–CO–CH_3) group in CS
2	Deacetylated chitosan (DCS)	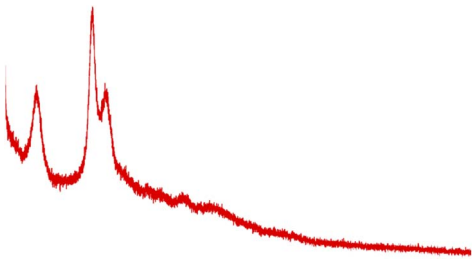	Destruction of the amide group (–NH–CO–CH_3), and responsible for amine group in DCS
3	*O*-Carboxymethyl chitosan Schiff base ligand	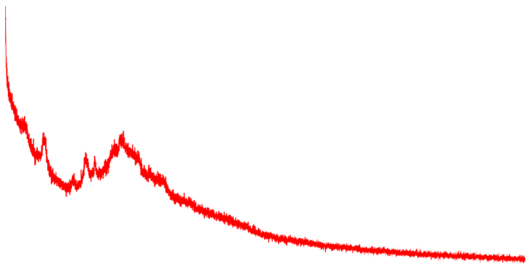	This indicates the strong incorporation of the Schiff base ligand (precursor) in the polymer backbone
4	*O*-CMCS metal complexes	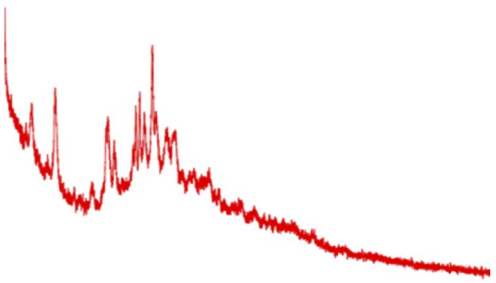	β-diketone and the π–π stacking with the metal ion, steric hindrance and hydrophobic interactions frequently reduce the crystal structure of the Schiff base ligand

intrinsic viscosity of the polymer decreases with increasing irradiation dose (kGy). The decrease in the molecular weight (M_w) is attributed to chain scission during depolymerization influenced by prolonged reaction time and strong alkali treatments.[26] The viscosity-average molecular weight of the chitosan was calculated and found to be approximately 85–90 kDa, and this shown in the SI as Fig. S1.

The UV-Visible spectrum of the Schiff base ligands exhibited two significant absorption bands at ~260 nm and ~310 nm. These peaks are attributed to the π–π* transition of the aromatic (C=C) groups and the n–π* transition of the imine (–C=N–) groups, respectively. The UV-Visible spectra of the *O*-CMCS Schiff base metal complexes of Co(II), Cu(II), and Zn(II) showed absorption around 750 nm. The observed shift of absorption toward higher wavelengths (red shift) is due to the d–d transition in the metal complexes. The formation of metal complexation is further confirmed by the shifts in the π–π* and n–π* transitions,[27] which shift to higher wavelengths (approximately 380 and 490 nm) due to the coordination between donor atoms (oxygen and nitrogen) present in the ligand.

The Fourier transform infrared (FT-IR) spectra of the biopolymer and their metal complex derivatives are shown in Fig. 1. A strong absorption band observed at 1590 cm^{-1}, corresponding to the amine group of chitosan, shifted to 1533 cm^{-1} after incorporation of the Schiff base ligand into the polymer backbone. This shift confirms the successful formation

Table 2 SEM images and their assignments of 4-bromo benzohydrazide, isoniazid, and 4-amino benzohydrazide-based biopolymer *O*-carboxymethyl chitosan Schiff base ligand and their Co(II), Cu(II), and Zn(II) complexes

Sl. no.	Biopolymer and its derivative	SEM image	Assignment
1	*O*-Carboxymethyl chitosan Schiff base ligand	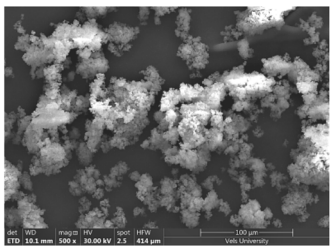	Condensation reaction occurs between Schiff base ligand and the polymer
2	*O*-CMCS-Co(OAc)$_2$	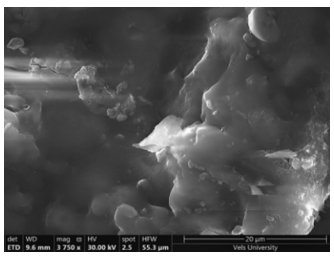	Complex formation between the ligand and cobalt metal tends to reduce the porous structure and the material changes into a uniform, layered surface
3	*O*-CMCS-Cu(OAc)$_2$	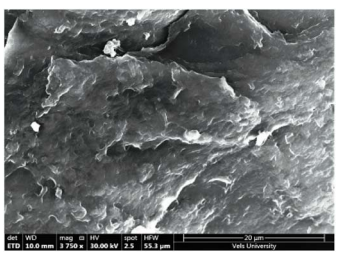	Complex formation between the ligand and copper metal tends to reduce the porous structure and the material changes into a uniform plain, layered surface
4	*O*-CMCS-Zn(OAc)$_2$	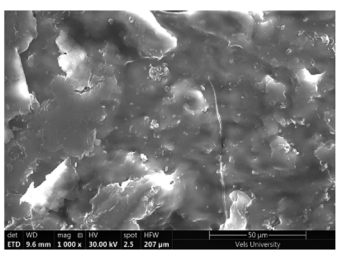	Complex formation between the ligand and zinc metal tends to reduce the porous structure and the material changes into a plain, smooth and layered surface

and coordination of the Schiff base within the polymeric matrix. The FT-IR spectra of the metal complexes are also represented in Fig. 1. Upon complexation, the wavenumber was extended ~1–15 cm^{-1}, indicating the coordination between the ligand and the metal ion. The observed bands for [OCMCS-Co(OAc)$_2$] are as follows: –OH and –NH stretching at 2925 cm^{-1} and 3411 cm^{-1}, respectively, –C=O (carboxyl) at 1709 cm^{-1}, –C=O (hydrazone) at 1623 cm^{-1}, –CH=N–(imine) at 1568 cm^{-1}, –C=O (acetate) at 1407 cm^{-1}, –C–N (hydrazone) at 1342 cm^{-1}, –N=NH stretching at 1026 cm^{-1}, and metal–ligand vibrations at 525 cm^{-1} (M–O) and 419 cm^{-1} (M–N) which are attributed to the coordination in the polymeric metal–ligand frame work.

The wave numbers of the copper metal complexes were observed as follows. [OCMCS-Cu(OAc)$_2$]: –C=O (carboxyl) at 1726 cm^{-1}, –C=O (hydrazone) at 1631 cm^{-1}, –CH=N– (imine) at 1577 cm^{-1}, 1409 cm^{-1}, >C=N–NH– (hydrazone) at 1378 cm^{-1}, –N=NH (stretching) at 1028 cm^{-1}, and M–O (complex) and M–N (complex) metal–ligand vibrations at 527 cm^{-1} and 413 cm^{-1}. The observed wave numbers for [OCMCS-Zn(OAc)$_2$] were as follows. –OH and –NH stretching at 2921 cm^{-1} and 3419 cm^{-1}, –C=O (carboxyl) at 1716 cm^{-1}, –C=O (hydrazone) at 1625 cm^{-1}, CH=N– (imine) at 1567 cm^{-1}, –C–N (hydrazone) at 1348 cm^{-1}, HN=N– (stretching) at 1024 cm^{-1}, and M–O (complex) and M–N (complex) metal–ligand vibrations at 523 cm^{-1} and 416 cm^{-1}.[28] The Raman spectrum of hydrazide-based *O*-carboxymethylchitosan Schiff base metal complex further confirms the coordination behavior. The vibrational modes between 400 and 700 cm^{-1} are attributed to the M–N and M–O coordination of the metal complexes. As shown in Fig. S2, the bands appearing at 357 cm^{-1} and 426 cm^{-1} indicate the M–O and M–N stretching vibrations, respectively, providing strong evidence of metal coordination through oxygen and the azomethine nitrogen atom. The band at 1083 cm^{-1} is assigned to the C–O–C stretching vibration of the glycosidic linkage of

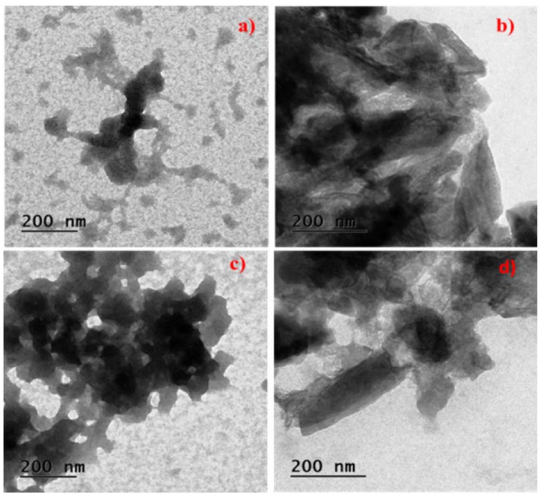

Fig. 2 TEM images of the (a) biopolymer *O*-carboxymethyl chitosan Schiff base ligand and its (b) Co(II), (c) Cu(II), and (d) Zn(II) complexes.

the polysaccharide back bone of chitosan. The peak observed at 1322 cm^{-1} corresponds to the amide band (C–N stretching), reflecting ligand framework vibrations influenced by metal coordination. The relatively limited number of observed peaks may be attributed to the Raman inactivity of several functional groups, as well as the amorphous nature of the biopolymeric network.[29]

The crystalline peaks of CS (90% deacetylated) were observed at $2\theta = 9°$, 12.05° and 20.14°. After complete deacetylation, the peaks shifted to $2\theta = 10.65°$ and 19.75° (Table 1). The Schiff base imine exhibited varying crystallinity indices, with maximum intensity in the range of $2\theta \approx 19–23°$ indicating an amorphous nature, and are represented in Table S1.

The aggregated peak at $2\theta = 23°$ shifted to $2\theta \approx 16°$, and new peaks appeared at $2\theta = 32°$ and 39°, indicating strong chelation between the tridentate ligand and the metal ion. The presence of β-diketone substituents and an electron rich π system along with metal π–π stacking, steric hindrance and hydrophobic interaction often reduce the crystal structure of the Schiff base ligand.[30] The percentage of crystalline indices of the polymer, ligands and their metal complexes were calculated using the following formula:

$$\text{Percentage of crystalline index} = \left[\frac{(1 - I_{am})}{I_{110}}\right] \times 100, \quad (3)$$

where I_{110} is the maximum intensity and I_{am} is the amorphous diffraction intensity. The overall order of the crystalline index for the various synthesized compounds is as follows:

CN > DCS > OCMCS > OCMCS-Co$(OAc)_2$ = OCMCS-Cu$(OAc)_2$ = OCMCS-Zn$(OAc)_2$. The X-ray diffractograms and the observed values of the biopolymer derivatives are represented in Table S3.

The SEM images of the polymer, ligands, and their derivatives show that the surface morphology of *O*-CMCS differs from that of the raw material due to the condensation reaction between the Schiff base ligand and the metal ion.[31] The complex formation tends to reduce the porous structure, resulting in a more uniform material with a layered surface. The morphological surfaces and assignments of the chitosan polymer derivatives are represented in Table 2. The EDAX spectrum confirms the formation of metal complexes through changes in the elemental composition, indicating the successful grafting of the metal ion onto the polymer. The elemental percentages of C, N, and O in the hydrazide-based Schiff base ligand decrease due to the metal ion incorporation.[32] The presence of elements such as C, N, O, Br, Cu, Co, and Zn further confirms the formation of metal complexes and the percentage of elements observed in the EDAX spectra for the metal complexes. The EDAX elemental compositions and elemental analyses of the polymer and its derivatives are represented in Tables S4a and b, respectively.

Fig. 2 displays the high-resolution transmission electron micrograph (HRTEM) images of the Schiff base ligand and its metal complexes. The average size of the Schiff base moieties (~10 nm) was determined through high-resolution transmission electron micrograph images. The Schiff base metal complex is comprised of bright spots, as shown in the TEM images. These bright spots suggest that the sample has a polycrystalline nature with preferential orientation in the crystalline domains of the metal complexes. The TEM micrographs further support a predominantly spherical morphology with some irregular moieties, and the presence of minor dark spots is attributed to the loaded metal ions on the hydrazide-incorporated Schiff base ligands. From the TEM analysis, it is

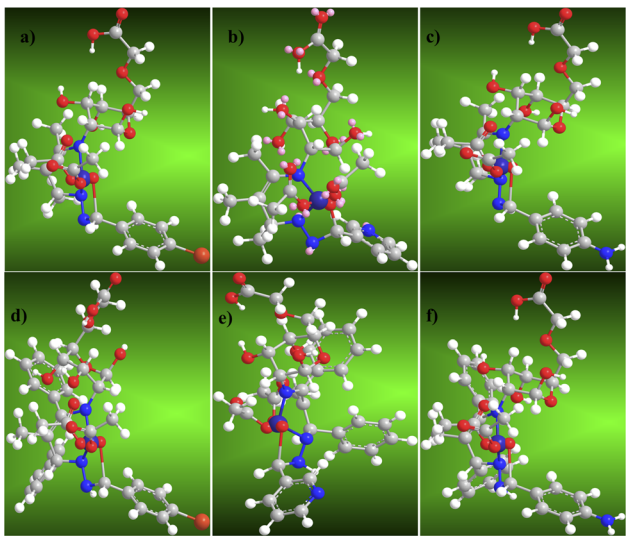

Fig. 3 Three-dimensional molecular structures of the Co(II) complexes with various Schiff bases showing their square pyramidal structures as confirmed by the selected bond lengths and bond angles. Three-dimensional molecular structures, selected bond lengths, and selected bond angles of the cobalt(II) metal complexes: (a) (IA-OCMCS-Co$(OAc)_2$) of the substituted hydrazide-incorporated 3-methylpentane-2,4-dione with the isoniazid of the Schiff base precursor (IA)-based biopolymer Schiff base ligand (IA-OCMCS), (b) (BHA-OCMCS-Co$(OAc)_2$), (c) (HBA-OCMCS-Co$(OAc)_2$), (d) (ID-OCMCS-Co$(OAc)_2$), (e) (BHD-OCMCS-Co$(OAc)_2$), and (f) (HBD-OCMCS-Co$(OAc)_2$). The atoms are highlighted in the coloured ball-stick model as follows: grey, Co; blue, N and red, O, using ChemDraw Professional version 16.0.

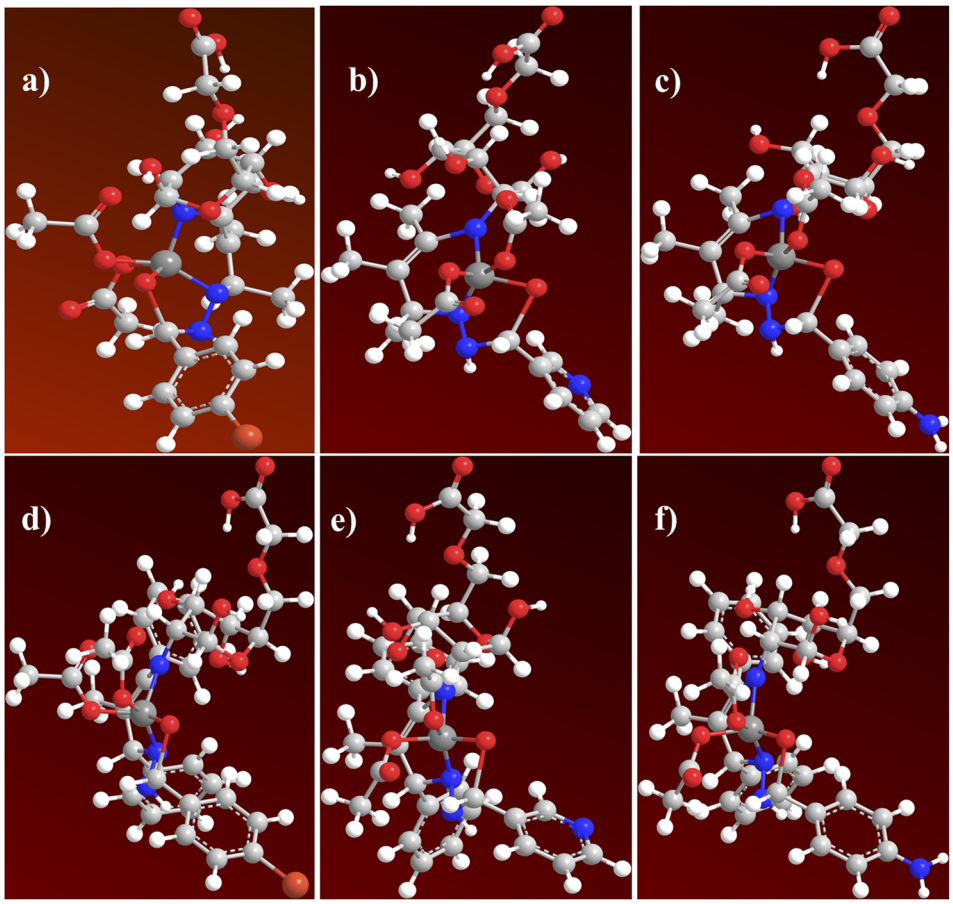

Fig. 4 Three-dimensional molecular structures, selected bond lengths, and selected bond angles of the Cu(II) metal complexes: (a) IA-OCMCS-$Cu(OAc)_2$, (b) BHA-OCMCS-$Cu(OAc)_2$, (c) HBA-OCMCS-$Cu(OAc)_2$, (d) ID-OCMCS-$Cu(OAc)_2$, (e) BHD-OCMCS-$Cu(OAc)_2$, and (f) HBD-OCMCS-$Cu(OAc)_2$.

observed that the Schiff base metal complexes consist of a thin shell over the metal core. The TEM images of the synthesized metal complexes reveal an average particle size range of ~53–58 nm, based on measurements of multiple particles from different regions of the micrograph.[33]

Nuclear magnetic resonance (NMR) studies were carried out for the prepared deacetylated chitosan (DCS) and synthesised novel hydrazone-based biopolymer Schiff base ligands, and the results are represented in Tables S5a and b. The ^{1}H-NMR chemical shift value (δ) of DCS showed no significant change from the functional groups of the prepared polymer. The ^{1}H-NMR peaks were observed at 2.00 ppm, indicating the acetyl group protons of the *N*-glucosamine unit. The ^{1}H-NMR chemical shift values (δ) of the synthesised hydrazone precursor incorporated Schiff base ligands (IA-OCMCS, BHA-OCMCS, HBA-OCMCS, Scheme: R_2-aliphatic group) were observed as follows: methyl (–CH_3) group protons at 1.91 3H(s), 2.22 3H(s), and 2.16 3H(s); methylene (–CH_2–) proton at 3.69 2H(s); imine (–N=C<) proton at 6.54 NH(s); aromatic protons at 8.55 H(s); hydrazone (>C=N–NH–) proton at 8.85 H(s); and carboxylic (–COOH) acidic proton at 10.45 H(s). Similarly, for the biopolymer Schiff base ligands (ID-OCMCS, BHD-OCMCS and HBD-OCMCS, Scheme: R_2-aromatic group), the values were as follows: methylene (–CH_2–) proton at 3.80 2H(s), imine (–N=C<) proton at 6.98 NH(s), aromatic protons at 7.84 H(s), hydrazone (>C=N–NH–) proton at 9.14 H(s), and carboxylic (–COOH) acidic proton at 11.36 H(s).[34]

The ^{13}C NMR chemical shift values (ppm) of IA-OCMCS, BHA-OCMCS, and HBA-OCMCS (Scheme: R_2-aliphatic group) were observed as follows: carbon of carboxymethyl moiety at 171.16 ppm, hydrazone (>C=N–NH–) carbon at 163.75 ppm, hydrazone (–N=C<) carbon at 173.97 ppm, imine (>C=N–) carbon at 145.67 ppm, aromatic ring carbon at 130.32 ppm and 129.88 ppm and methylene (–CH_2) carbon at 39.73 ppm. The ^{13}C NMR chemical shift values of ID-OCMCS, BHD-OCMCS and HBD-OCMCS (Scheme: R_2-aromatic group) were observed as follows: carbon of carboxymethyl moiety at 191.43 ppm, hydrazone (>C=N–NH–) carbon at 181.26 ppm, hydrazone (–N=C<) carbon at 180.98 ppm, imine (>C=N–) carbon at 156.65 ppm, aromatic ring carbon at 130.95 and 131.25 ppm and methylene (–CH_2) carbon at 42.48 ppm.[35]

3.3 Selected bond lengths and bond angles of cobalt complexes

The interatomic distances (d) (bond length (Å)) and bond angles (°) for the metal complex were determined and are shown in

Fig. 3a–f. The cobalt metal ion had a five-coordinated structure through two acetates and three bridging coordinations of nitrogen, nitrogen, and oxygen from the tridentate ligands. The coordination geometry is identified as square pyramidal according to the bond distances between the metal and donor atoms. The Co–N bonds of the cobalt metal complexes were longer (1.842 Å) than the Co–O bonds (0.600 Å).

Because of Jahn–Teller distortion, high-spin complexes of cobalt exhibit a large difference in the Co–N bond lengths in the equatorial and axial positions which cannot be explained further. The bromine-substituted hydrazide ring extended the bond length from 1.509 Å to 1.881 Å due to the lone pair of electrons present in the bromine atom. The bond length (1.352 Å) of the hydrazone linkage (N(17)–N(19)) of the Schiff base ligand was extended after the cobalt metal complexation.[36] Selected bond lengths and bond angles of the Co(II) metal complexes are shown in Table S6a.

3D models (Fig. 4) of the prepared compounds and selected bond lengths and bond angles of the Cu(II) metal complexes of Schiff base ligands IA-OCMCS, BHA-OCMCS, HBA-OCMCS, ID-OCMCS, BHD-OCMCS, and HBD-OCMCS are represented in Table S6b.

The copper and oxygen atoms of hydrazide (Cu(28)–O(49)) have a molecular bonding length of 1.810 Å; the bond angle for the same coordination (C(47)–O(45)–Cu(28)) was 120.000°. For the bond of Cu(28)–O(49), the oxygen atom of hydrazide pulls towards itself, leading to an extension of the bond length of the central metal copper to the oxygen atom of hydrazide. The bond length of the imine linkage (N(8)–C(13)) was observed to be within an optimal range at 1.438 Å. The imine linkages (Cu(39)–N(17)) with the bond angles of 89.999° to the copper complexes reveal that the copper metal complexes possess a square pyramidal geometry.[37]

3D models (Fig. 5) of the prepared compounds and selected bond distances and bond angles of the zinc-incorporated *O*-carboxymethyl chitosan Schiff base metal complexes are represented in Table S6c. The bond length of the zinc ester linkage (Zn(28)–O(49)) was observed to be 1.890 Å, and the bond angle C(51)–O(49)–Zn(28) was found to be 120.000°; this reveals that the acetate molecule of the complex is strongly coordinated with the zinc metal. The bond length of the zinc-imine functionality (N(17)–Zn(39)) was observed to be 1.842 Å for the zinc metal complexes, and the bond angle of the imine coordinated zinc metal complexes (O(50)–Zn(39)–N(17)) was 89.999°; this indicates that the geometry of the complexes was square pyramidal.[38] The zinc metal ion is penta-dentate to the hydrazone-based polymer Schiff base ligands and possesses a distorted square pyramidal geometry. The imine linkage (N(8)–C(13)) of the metal complexes stretched the bond length to 1.647 Å. This could be due to the electron-withdrawing interaction (pulling action) of the imine nitrogen donor on the zinc metal ion.[39] In all cobalt(II), copper(II), and zinc(II) metal complexes, the bromine (C(3)–Br(29)) and methoxy-substituted (C(3)–O(27)) hydrazide bond lengths were observed to be 1.881 Å and 1.355 Å, respectively.

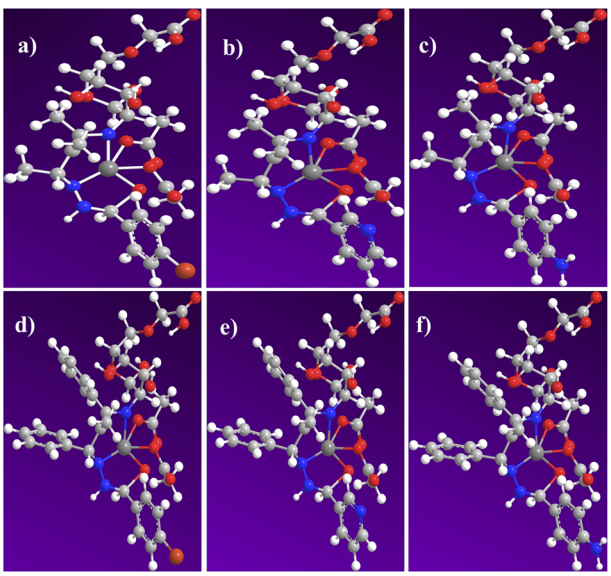

Fig. 5 3D molecular structures, selected bond lengths, and selected bond angles of the zinc(II) metal complexes: (a) IA-OCMCS-Zn$(OAc)_2$, (b) BHA-OCMCS-Zn$(OAc)_2$, (c) HBA-OCMCS-Zn$(OAc)_2$, (d) ID-OCMCS-Zn$(OAc)_2$ of the substituted hydrazide-based biopolymer Schiff base ligand (ID-OCMCS), (e) BHD-OCMCS-Zn$(OAc)_2$, and (f) HBD-OCMCS-Zn$(OAc)_2$. The 3D molecular structures of the Zn(II) complexes are represented in the coloured ball-stick model as follows: grey, Zn; blue, N and red, O atoms, using ChemDraw Professional version 16.0.

3.4 Antibacterial analysis

The antibacterial analysis of the synthesized metal compounds was performed using the following pathogens and the reference drug ampicillin by the Kirby–Bauer disk diffusion method. (a) *Escherichia coli*, (b) *Pseudomonas aeruginosa*, (c) *Staphylococcus aureus*, and (d) *Bacillus subtilis* were selected due to their relevance in the pharmaceutical, biomedical, and clinical fields. Some of the hydrazone-incorporated metal complexes enhanced bactericidal action and exhibited better results than our previously reported findings, as supported by the literature.[40] In this present investigation, the bacterial organism *B. subtilis* did not show significant sensitivity towards [OCMCS-Co$(OAc)_2$].

Water and DMSO were taken as control I and control II, respectively, and neither solvent showed any significant bacterial effect. The Co(II) metal complexes exhibited comparatively low bactericidal action against *B. subtilis*. The exhibited bacterial growth inhibitions of the metal complexes were as follows: [OCMCS-Zn$(OAc)_2$] ~34 mm, [OCMCS-Cu$(OAc)_2$] ~30 mm, and [OCMCS-Co$(OAc)_2$] ~24 mm. This could be attributed to *B. subtilis* being a Gram +ve microorganism frequently encountered in the environment.

Overall, the antibacterial results of the prepared metal complexes demonstrated significant antibacterial effects, evidenced by the measurable zones of inhibition that confirm their effective bactericidal activities against pathogens.[41] For example, the Gram +ve pathogen *S. aureus* at 250 μg μL^{-1} requires 24 times the amount of ampicillin (standard drug) to

Table 3 *In vitro* antibacterial activities (MIC, μg μL^{-1}) of the *O*-CMCS Schiff bases, their Co(II), Cu(II), and Zn(II) complexes and the standard drug ampicillin

Name of the compound	Bacterial growth inhibition (mm)							
	E. coli (Gram −ve)		*P. aeruginosa* (Gram −ve)		*S. aureus* (Gram +ve)		*B. subtilis* (Gram +ve)	
	Minimum and maximum concentration (μg μL^{-1})							
	50	**250**	**50**	**250**	**50**	**250**	**50**	**250**
IA-OCMCS	5 ± 0.25	18 ± 0.4	7 ± 0.3	23 ± 0.6	6 ± 0.3	20 ± 0.5	4 ± 0.2	21 ± 0.5
[(IA-OCMCS)-Co(OAc)$_2$]	6 ± 0.3	28 ± 0.7	14 ± 0.7	31 ± 1.4	12 ± 0.6	24 ± 0.6	8 ± 0.3	24 ± 0.5
[(IA-OCMCS)-Cu(OAc)$_2$]	8 ± 0.3	26 ± 0.6	9 ± 0.3	34 ± 1.5	10 ± 0.4	36 ± 1.4	7 ± 0.3	30 ± 1.1
[(IA-OCMCS)-Zn(OAc)$_2$]	9 ± 0.4	30 ± 0.8	10 ± 0.4	36 ± 1.7	13 ± 0.6	34 ± 1.2	8 ± 0.3	34 ± 1.4
BHA-OCMCS	6 ± 0.25	24 ± 0.5	4 ± 0.15	17 ± 0.4	6 ± 0.3	25 ± 0.5	5 ± 0.2	24 ± 0.5
[(BHA-OCMCS)-Co(OAc)$_2$]	7 ± 0.3	25 ± 0.5	5 ± 0.2	19 ± 0.4	8 ± 0.35	29 ± 1	7 ± 0.3	26 ± 0.5
[(BHA-OCMCS)-Cu(OAc)$_2$]	7 ± 0.3	24 ± 0.5	5 ± 0.2	20 ± 0.5	10 ± 0.5	38 ± 1.5	9 ± 0.4	25 ± 0.5
[(BHA-OCMCS)-Zn(OAc)$_2$]	9 ± 0.4	27 ± 0.7	7 ± 0.3	25 ± 0.5	13 ± 0.7	40 ± 2	11 ± 0.6	34 ± 1.4
HBA-OCMCS	7 ± 0.3	19 ± 0.4	4 ± 0.2	21 ± 0.5	6 ± 0.3	23 ± 0.5	5 ± 0.2	20 ± 0.4
[(HBA-OCMCS)-Co(OAc)$_2$]	14 ± 0.7	36 ± 1.6	9 ± 0.5	31 ± 1.0	13 ± 0.7	32 ± 1	8 ± 0.3	24 ± 0.6
[(HBA-OCMCS)-Cu(OAc)$_2$]	11 ± 0.6	30 ± 0.8	10 ± 0.5	32 ± 1.3	12 ± 0.6	36 ± 1.6	6 ± 0.3	28 ± 0.7
[(HBA-OCMCS)-Zn(OAc)$_2$]	9 ± 0.5	34 ± 1.2	8 ± 0.4	34 ± 1.4	10 ± 0.5	28 ± 0.7	7 ± 0.3	30 ± 0.8
ID-OCMCS	2 ± 0.1	19 ± 0.4	6 ± 0.3	22 ± 0.5	5 ± 0.25	18 ± 0.4	3 ± 0.2	15 ± 0.3
[(ID-OCMCS)-Co(OAc)$_2$]	6 ± 0.3	28 ± 0.7	14 ± 0.6	31 ± 1.1	9 ± 0.45	26 ± 0.7	6 ± 0.3	19 ± 0.4
[(ID-OCMCS)-Cu(OAc)$_2$]	7 ± 0.3	26 ± 0.6	10 ± 0.5	33 ± 1.3	11 ± 0.5	36 ± 1.5	7 ± 0.3	22 ± 0.5
[(ID-OCMCS)-Zn(OAc)$_2$]	9 ± 0.45	25 ± 0.5	12 ± 0.6	37 ± 1.7	14 ± 0.6	30 ± 0.8	8 ± 0.3	26 ± 0.7
BHD-OCMCS	4 ± 0.2	20 ± 0.5	2 ± 0.1	9 ± 0.2	3 ± 0.2	12 ± 0.3	2 ± 0.1	10 ± 0.2
[(BHD-OCMCS)-Co(OAc)$_2$]	5 ± 0.2	22 ± 0.5	3 ± 0.2	12 ± 0.3	4 ± 0.2	19 ± 0.5	5 ± 0.2	20 ± 0.5
[(BHD-OCMCS)-Cu(OAc)$_2$]	6 ± 0.3	23 ± 0.5	5 ± 0.2	17 ± 0.5	6 ± 0.3	24 ± 0.5	7 ± 0.3	21 ± 0.5
[(BHD-OCMCS)-Zn(OAc)$_2$]	9 ± 0.4	30 ± 1	7 ± 0.3	28 ± 1	7 ± 0.3	25 ± 0.5	8 ± 0.3	28 ± 1
HBD-OCMCS	4 ± 0.25	16 ± 0.3	2 ± 0.1	10 ± 0.2	6 ± 0.3	18 ± 0.4	3 ± 0.1	15 ± 0.3
[(HBD-OCMCS)-Co(OAc)$_2$]	8 ± 0.35	18 ± 0.4	5 ± 0.25	15 ± 0.3	9 ± 0.45	26 ± 0.6	6 ± 0.3	18 ± 0.4
[(HBD-OCMCS)-Cu(OAc)$_2$]	12 ± 0.6	21 ± 0.5	8 ± 0.35	19 ± 0.4	14 ± 0.6	38 ± 1.6	7 ± 0.3	22 ± 0.5
[(HBD-OCMCS)-Zn(OAc)$_2$]	9 ± 0.45	23 ± 0.7	9 ± 0.45	24 ± 0.5	11 ± 0.5	34 ± 1.4	9 ± 0.3	26 ± 0.7
Ampicillin (10 μg μL^{-1})	4 ± 0.2	24 ± 0.5	3 ± 0.15	21 ± 0.5	8 ± 0.4	24 ± 0.6	4 ± 0.2	25 ± 0.5
Water (control-I)	—	—	—	—	—	—	—	—
DMSO (control-II)	1 ± 0.2	1 ± 0.2	1 ± 0.2	2 ± 0.2	1 ± 0.1	3 ± 0.2	1 ± 0.15	2 ± 0.15

reach the efficacy of [OCMCS-Co(OAc)$_2$] and [OCMCS-Cu(OAc)$_2$]; [OCMCS-Zn(OAc)$_2$] produced 26 mm of bactericidal effect, and, in addition to that, it extended the growth inhibition up to 8 mm wider than [OCMCS-Co(OAc)$_2$] and showed better bactericidal resistance against *S. aureus*. The scavenging efficiency for *E. coli* was compared for the synthesized Co(II), Cu(II), and Zn(II) metal complexes, and the obtained results did not show better activity in the *E. coli* bacterial field. The synthesized novel metal complexes showed better bacterial action on the microorganism *P. aeruginosa*. Ampicillin was used as the standard drug for the entire antimicrobial study.

Although only minor differences were observed in the antibacterial results, [OCMCS-Zn(OAc)$_2$] exhibited the predominant effect against the *P. aeruginosa* bacterial field, while [OCMCS-Co(OAc)$_2$] showed slightly less effect than [OCMCS-Cu(OAc)$_2$]. The prepared biopolymer *O*-CMCS Schiff base metal complexes scavenged well on the bacterial field, with 37 ± 1.7 mm, 33 ± 1.3 mm and 31 ± 1.1 mm maximum bacterial growth inhibitions at 250 mg mL^{-1} for [(ID-OCMCS)-Zn(OAc)$_2$], [(ID-OCMCS)-Cu(OAc)$_2$] and [(ID-OCMCS)-Co(OAc)$_2$], respectively. The antibacterial results for the synthesized metal complexes are given in Table 3. Furthermore, it was observed that the total bacterial count decreased progressively with increasing concentrations of [ID-OCMCS-Zn(OAc)$_2$], indicating enhanced antibacterial effect at higher concentrations of antibacterial agent.[42]

This effect might be due to the active bromine atom of the metal complexes with aromatic compounds. The *S. aureus* bacterial field had significant inhibition compared with that of *E. coli* under the same concentration conditions. The observed differences in antibacterial activity may be attributed to variation in bacterial cell walls, particularly the presence of polyglycogen, which is the major constituent of the *S. aureus* cell wall. The antibacterial effects of the compounds are illustrated in Fig. 6. Due to the presence of peptidoglycan pores, the ID-OCMCS-Zn(OAc)$_2$ Schiff base metal complex can effectively penetrate the cell wall, thereby enhancing the cellular uptake and facilitating bacterial cell disruption. In contrast, cell wall of *E. coli* is made of a thin, negatively charged peptidoglycan surrounded by an outer membrane of lipopolysaccharides, lipoproteins, and phospholipids, so the prepared antibacterial agents stop further replication. This bactericidal action could involve disruption of the bilayer membrane and subsequent cell wall damage.[40,41]

3.4.1 Mechanistic insights into the antimicrobial actions of biopolymer–metal complexes and oxidative stress due to ROS generation. Most antimicrobial drugs act on bacteria by inhibiting the synthesis of the cell wall (with peptidoglycan as the

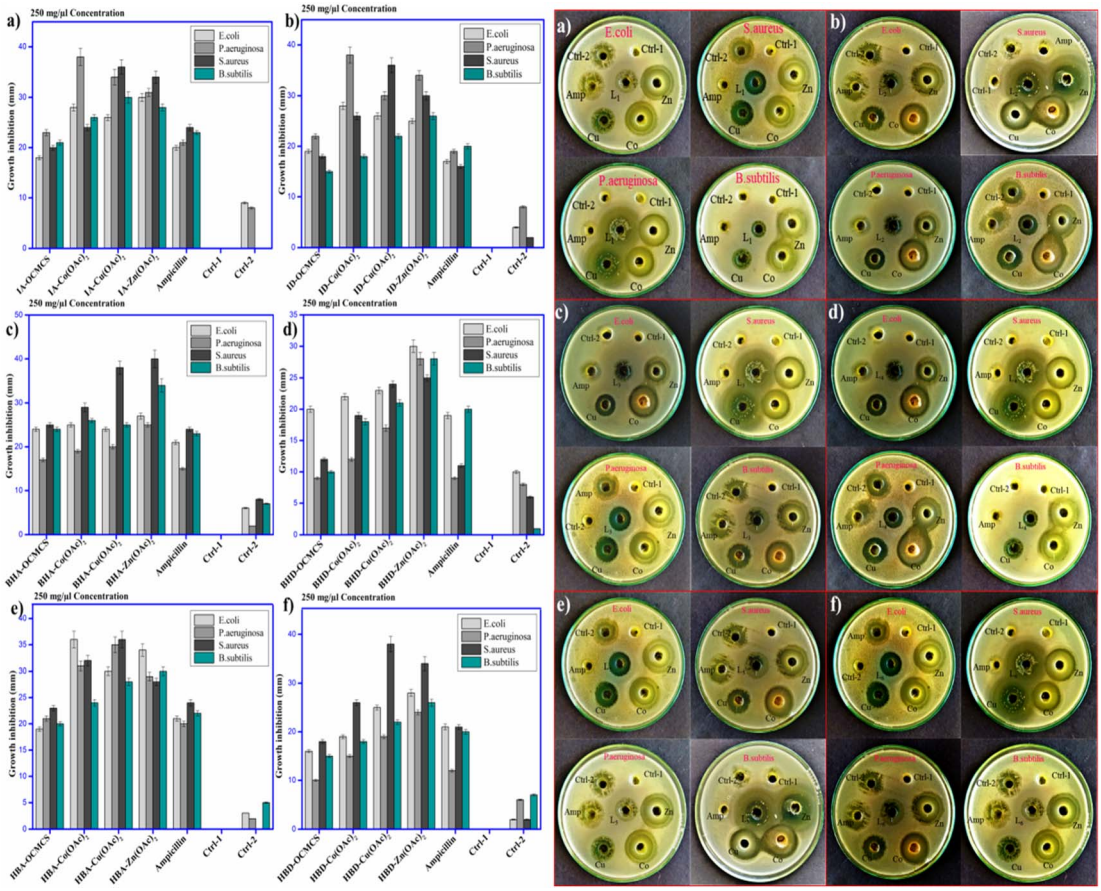

Fig. 6 Bactericidal actions shown in Petri dishes and with bar charts against *E. coli*, *P. aeruginosa*, *S. aureus*, and *B. subtilis* for the synthesised biopolymer Schiff bases and their Zn(II) metal complexes, with sample dosages of 50 mg mL^{-1} and concentrations of 250 mg mL^{-1}, ampicillin as reference, and water as control, better than those of other metal complexes. Antibacterial activity of the prepared hydrazide-based (a) biopolymer/*O*-carboxymethyl chitosan (IA-OCMCS), (b) ID-OCMCS, (c) BHA-OCMCS, (d) BHD-OCMCS, (e) HBA-OCMCS, and (f) HBD-OCMCS Schiff bases and their respective Co(II), Cu(II), and Zn(II) metal complexes.

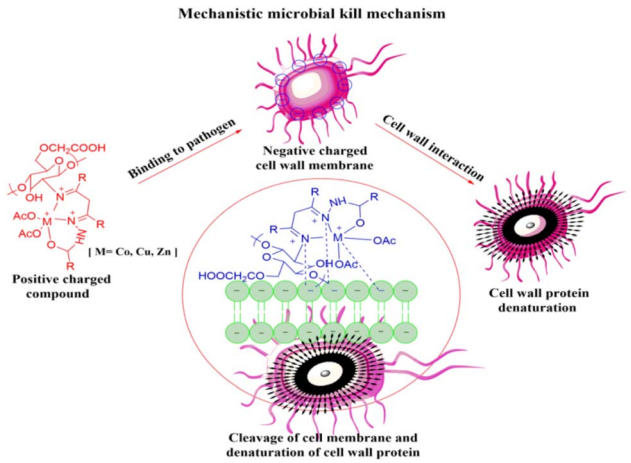

Fig. 7 Mechanistic cell wall cleavage and denaturation of cell wall proteins. The thin negatively charged membrane, the peptidoglycan component of the cell membrane and the outer membranes of lipopolysaccharides, lipoproteins, and phospholipids attribute to the microbial action through complexity between the bilayer cell and the prepared biopolymer metal complexes, which destroy the cell wall of the pathogen.

primary target), nucleic acid synthesis and protein synthesis and by modification of the membrane permeability. Bacteria are adept at developing or acquiring resistance mechanisms that are independent of these target functionalities. Cell wall modifications arise due to expression by the antimicrobial agents of enzymes capable of altering or degrading the cell wall, as well as ribosomal mutations that prevent antibiotic binding. Additionally, change in porin expression with or without an active efflux mechanism to resistance. These mechanisms can be induced or enhanced during reactive oxygen species (ROS) stress and the proposed mechanistic cell wall cleavage and protein denaturation illustrated below in Fig. 7.[43,44]

The use of metal complexes as antibacterial agents has opened new avenues to combating antimicrobial resistance. More evidence suggests that the metal complexes act effectively on bacterial cell walls, though the antibacterial mechanisms are not fully elucidated. It has been noted that Gram-positive and Gram-negative cell walls promote interaction between the metal complexes and the negatively charged molecules composing the bacterial cell membrane. These negatively charged molecules of the bacterial cell membrane strongly hold the positive ions released by the metal complexes through electrostatic attraction

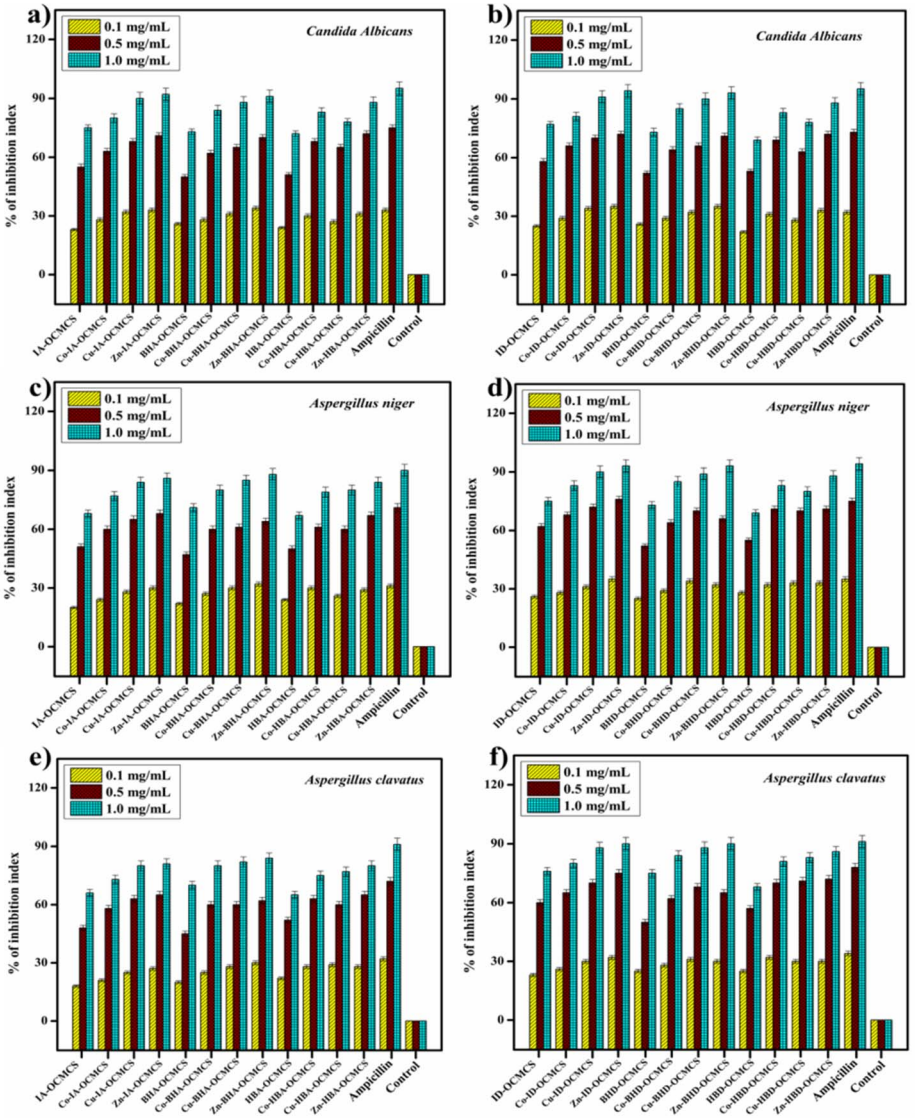

Fig. 8 Antifungal activities of the prepared Schiff base ligands (a) IA-OCMCS, (b) BHA-OCMCS, (c) HBA-OCMCS, (d) ID-OCMCS, (e) BHD-OCMCS, and (f) HBD-OCMCS and their Co(II), Cu(II), and Zn(II) metal complexes against various fungal fields (*Candida albicans*, *Aspergillus niger*, and *Aspergillus clavatus*) with sample dosages of 0.1 mg mL^{-1}, 0.5 mg mL^{-1}, and 1.0 mg mL^{-1} as concentrations, ampicillin as reference, and water as control. The antifungal analysis with the bar chart diagrams shows better efficacies in *Candida albicans* than other fungal species for the prepared compounds.

on the bacterial surface, which induces cell wall disruption and an increase in its permeability. This, in turn, affects the metabolic pathways and effects changes in membrane shape and function. A positively charged metal ion inhibits enzymes, deactivates proteins, and induces oxidative stress and electrolyte imbalance at the reactive centre, disrupting biological processes once it enters the cells.[45,46] Of these prepared Schiff base metal complexes, the Zn-inserted biopolymer hydrazide incorporated N, N, O donor tridentate metal complexes exhibited the maximum scavenging activities in the bacterial field. Furthermore, these complexes effectively disrupted well, though the components of the cell membrane were a thick peptidoglycan (Gram +ve) without an outer membrane and a thin peptidoglycan (Gram −ve) layer with an outer membrane of the bacterial cell wall.

Fig. 7 illustrates the antibacterial processes and mechanisms for the metal ions. The metal complexes adhere to and penetrate the cell wall through electrostatic interaction. Owing to this, the cell wall and membrane are disrupted, leaking the intracellular materials, such as ribosomes, DNA (in a nucleoid), plasmids, and enzymes, existing within the cytoplasm of the bacterial cell. Furthermore, homeostasis is disrupted because of the cytoplasm leakage. Reactive oxygen species (ROS) can penetrate the bacterial cell wall and plasma membrane, including the nucleoid region, causing the cleavage and denaturation of cell proteins by ROS-induced damage. Moreover, the overall mechanism of ROS leads to the disruption of DNA and other vital biomolecules.

3.5 Antifungal activities

The antifungal activities of the polymer and its complex derivatives are presented in Fig. 8a–f. The synthesized biopolymer ligands and their [OCMCS-Co(OAc)$_2$], [OCMCS-Cu(OAc)$_2$], and [OCMCS-Zn(OAc)$_2$] metal complexes were evaluated against fungi such as *A. niger*,*C. albicans*, and *A. clavatus*. The antifungal efficacies of the biopolymer ligands and their metal complexes were compared with that of ampicillin; the results showed that the Zn(II) metal complexes of the biopolymer exhibited superior fungicidal action, particularly against *Candida albicans* compared to other pathogens. Chitosan shows poor solubility in water; however, structural modification through carboxymethylation and hydrazone formation enhances its water-soluble nature, thereby improving the antifungal efficacies. According to literature reports, chitosan-based metal complexes exhibit better antifungal activity than raw chitosan.[47] This enhancement may be attributed to surface interaction between the positively charged metal complexes and negatively charged components of the fungal cell wall. The order of fungicidal activity of the hydrazide-based biopolymer ligands and their complex derivatives at concentrations of 0.1, 0.5, 1.0 mg mL^{-1} was evaluated in triplicate, and the results are as follows: *C. albicans* > *A. niger* > *A. clavatus*.

The zinc metal complexes of the biopolymer Schiff bases inhibited the fungal growth completely at all test concentrations. As shown in Fig. 8, *O*-carboxymethyl chitosan and its derivatives exhibit better antifungal activity at all tested concentrations against *Candida albicans.* Furthermore, the fungal growth inhibition of all samples increases with increase in concentration.[48] The antifungal activities of raw chitosan, the synthesised Schiff base ligands, and their Co(II), Cu(II), and Zn(II) metal complexes showed an inhibitory index of less than 32.0% at 0.1 mg mL^{-1} in *Aspergillus niger* and *Aspergillus clavatus*. The Zn(II) metal complexes exhibited better antifungal activity than chitosan and their corresponding Cu(II) and Co(II) metal complexes. The inhibitory indices of *Candida albicans* at 1.0 μg mL^{-1} (dosage) were 91.6% (Zn-IA-OCMCS), 90.9% (Zn-BHA-OCMCS), 89.1% (Zn-HBA-OCMCS), 92.8% (Zn-ID-OCMCS), 92.3% (Zn-BHD-OCMCS), and 88.9% (Zn-HBD-OCMCS). Similarly, for *Aspergillus niger*, the values were 88.6%, 89.8%, 86.1%, 91.6%, 90.9%, and 86.9%, respectively, while for *Aspergillus clavatus*, the corresponding values were 81.3%, 83.6%, 79.1%, 89.8%, 88.9%, and 82.5% at the same concentrations.[49]

The enhanced antifungal activity of the prepared Schiff base metal complexes is attributed to the interaction between the positively charged metal ion and negatively charged components of the fungal cell membrane. Furthermore, the antifungal results confirm that hydrazone-grafted *O*-CMCS Schiff base derivatives exhibit improved antifungal action, particularly at higher concentrations (1.0 mg mL^{-1}).

The hydrophobic moiety of the synthesized *O*-CMCS Schiff base derivatives influences fungal growth, and these compounds could be used as efficient bactericides and fungicides. This antimicrobial study reveals that Zn(II) metal complexes exhibit a significant synergistic effect on antimicrobial activity.

4 Conclusion

In summary, the accumulation of lobster shell waste makes huge deposits. To address this issue, a value-added product, chitin, was successfully extracted from the waste heaps through a green approach involving demineralization and deproteinization under mild acid–base treatment. The degree of deacetylation of the resulting polymer was achieved in the range of 80–90%. The porosity (ϕ) of the Co(II) metal complexes was found to be higher than those of the Cu(II) and Zn(II) metal complexes. FT-IR spectral analysis confirmed the successful formation of chitosan polymer, Schiff base ligands, and their corresponding metal complexes. The crystallinity indices of the Schiff base compounds decreased significantly, indicating disruption of the polymer crystalline structure upon metal complexation. SEM images revealed that the prepared metal complexes showed a uniform, layered morphology distinct from the raw chitosan, Schiff base ligands, and corresponding metal complexes. Furthermore, 3D modeling of the synthesised biopolymer metal complexes confirmed the presence of the functional group and the substituent within the polymer framework. The geometry of the metal complexes was validated through bond length and bond angle measurements of the biopolymer derivatives. Antibacterial studies demonstrated that the Schiff base ligands and their metal complexes, particularly the Co(II) and Zn(II) complexes, showed significant growth inhibition zones of 38 ± 2 mm and 36 ± 2 mm, respectively. Additionally, this study provides a foundation for further exploration into secondary lymphedema treatment. The findings suggest potential applications in activating fibroblasts—cells responsible for extracellular matrix (ECM) production—through transforming growth factor signaling pathways.

Statistical analysis

The statistical analysis was carried out using the zone inhibition method, and the level of significance was evaluated at $p < 0.05$. All experiments were performed in triplicate ($n = 3$). Data are expressed as mean ± standard deviation.

Author statement

Murugaiyan Manimohan: research idea conceptualization, methodology, study planning, data analysis, manuscript writing – review and editing and Mohamed Aboobucker Sithique: manuscript review, methodology, data curation, validation and investigation. All authors read and approved the final manuscript. Sivashanmugam Pugalmani: modified manuscript – data curation, validation, and investigation.

Conflicts of interest

The authors declare that they have no known competing financial interests or personal relationships that could have appeared to influence the work reported in this paper.

Abbreviations

CN	Chitin
CS	Chitosan
O-CMCS	*O*-Carboxymethylchitosan
LMw	Low molecular weight
DCS	Deacetylated chitosan
FT-IR	Fourier transform infrared
UV-Vis	Ultraviolet visible
XRD	X-ray diffraction
SEM	Scanning electron microscopy
EDAX	Energy dispersive X-ray analysis
3D	Three dimensional
DMF	Dimethyl formamide
DMSO	Dimethyl sulphoxide
kDA	Kilodaltons
PDA	Potato dextrose agar
MHA	Mueller–Hinton agar
SDA	Sabouraud dextrose agar
ICP-OES	Inductively coupled plasma-optical emission spectrometry
NMR	Nuclear magnetic resonance
IA	3-Methylpentane-2,4-dione with isoniazid of the Schiff base precursor
BHA	3-Methylpentane-2,4-dione with 4-bromobenzohydrazide of the Schiff base precursor
HBA	3-Methylpentane-2,4-dione with 4-aminobenzohydrazide of the Schiff base precursor
ID	2-Methyl-1,3-diphenylpropane-1,3-dione with isoniazid of the precursor
BHD	2-Methyl-1,3-diphenylpropane-1,3-dione with 4-bromobenzohydrazide of the precursor
HBD	2-Methyl-1,3-diphenylpropane-1,3-dione with 4-aminobenzohydrazide of the precursor
ECM	Extracellular matrix

Data availability

Data will be made available upon request.

Supplementary information (SI): reinforcement of characterisation studies for the prepared compounds. See DOI: https://doi.org/10.1039/d6ra00600k.

References

1 M. Manimohan and S. Pugalmani, Synthesis and characterisation of novel Cu (II)-anchored biopolymer complexes as reusable materials for the photocatalytic degradation of methylene blue, *RSC Adv.*, 2020, **10**, 18259–18279, DOI: 10.1039/D0RA01724H.

2 S. S. Silva and J. F. Mano, Ionic liquids in the processing and chemical modification of chitin and chitosan for biomedical applications, *Green Chem.*, 2017, **19**(5), 1208–1220, DOI: 10.1039/c6gc02827f.

3 K. Mohan and S. Ravichandran, Extraction and characterization of chitin from sea snail Conus inscriptus (Reeve, 1843), *Int. J. Biol. Macromol.*, 2018, **126**, 555–560, DOI: 10.1016/j.ijbiomac.2018.12.241.

4 H. S. Adhikari and P. N. Yadav, Anticancer activity of chitosan, chitosan derivatives, and their mechanism of action, *Int. J. Biomater.*, 2018, 1–29, DOI: 10.1155/2018/2952085.

5 C.-L. Ke and F.-S. Deng, Antimicrobial Actions and Applications of Chitosan, *Polym*, 2021, **13**(6), 904, DOI: 10.3390/polym13060904.

6 K. Muraleedharan and C. H. Viswalekshmi, Synthesis, characterization and thermal dehydration and degradation kinetics of chitosan Schiff bases of o-, m- and p-nitrobenzaldehyde, *Polym. Bull.*, 2016, **74**(1), 39–54, DOI: 10.1007/s00289-016-1696-1.

7 R. A. Abdel-Monem and A. M. Khalil, Antibacterial properties of carboxymethyl chitosan Schiff-base nanocomposites loaded with silver nanoparticles, *J. Macromol. Sci., Part A: Pure Appl. Chem.*, 2019, 1–11, DOI: 10.1080/10601325.2019.1674666.

8 D. Egli and R. Baumann, Structural characteristics, bulk porosity and evolution of an exhumed long-lived hydrothermal system, *Tectonophysics*, 2018, **747–748**, 239–258, DOI: 10.1016/j.tecto.2018.10.008.

9 Z. Jiang and Y. Song, Rat sciatic nerve regeneration across a 10-mm defect bridged by a chitin/CM-chitosan artificial nerve graft, *Int. J. Biol. Macromol.*, 2019, **129**, 997–1005, DOI: 10.1016/j.ijbiomac.2019.02.080.

10 H. Srinivasan and V. Kanayairam, Chitin and chitosan preparation from shrimp shells Penaeus monodon and its human ovarian cancer cell line, PA-1, *Int. J. Biol. Macromol.*, 2018, **107**, 662–667, DOI: 10.1016/j.ijbiomac.2017.09.035.

11 M. Kaya and Y. S. Cakmak, New chitin, chitosan, and O-carboxymethyl chitosan sources from resting eggs of Daphnia longispina (Crustacea); with physicochemical characterization, and antimicrobial and antioxidant activities, *Biotechnol. Bioprocess Eng.*, 2014, **19**(1), 58–69, DOI: 10.1007/s12257-013-0488-9.

12 W. Liu and Y. Qin, C-coordinated O -carboxymethyl chitosan metal complexes: Synthesis, characterization and antifungal efficacy, *Int. J. Biol. Macromol.*, 2018, **106**, 68–77, DOI: 10.1016/j.ijbiomac.2017.07.176.

13 N. A. Anan and S. M. Hassan, Preparation, characterization and pH-metric measurements of 4-hydroxysalicylidenechitosan Schiff-base complexes of Fe(III), Co(II), Ni(II), Cu(II), Zn(II), Ru(III), Rh(III), Pd(II) and Au(III), *Carbohydr. Res.*, 2011, **346**(6), 775–793, DOI: 10.1016/j.carres.2011.01.014.

14 A. Hari Sharan and G. Aditya, Pyridine-Based NNS Tridentate Chitosan Thiosemicarbazones and Their Copper(II) Complexes: Synthesis, Characterization, and Anticancer Activity, *ACS Omega*, 2022, **7**, 30978–30988, DOI: 10.1016/j.msec.2017.03.198.

15 M. Ali and E. N. Sholkamy, Synthesis of Schiff Bases Based on Chitosan and Heterocyclic Moiety: Evaluation of Antimicrobial Activity, *ACS Omega*, 2023, **8**, 47304–47312, DOI: 10.1021/acsomega.3c08446.

16 D. Venkata Padmaja and H. R. Rajegowda, New thioether-hydrazide based ONS donor Schiff base and its Pd(II) complex: Synthesis, crystal structure, thermal analysis, hirshfeld surface analysis, quantum chemical studies and molecular docking, *J. Mol. Struct.*, 2023, **1281**, 135041, DOI: 10.1016/j.molstruc.2023.135041.

17 Z. Jie and F. Mi, Base-free preparation of low molecular weight chitin from crab shell, *Carbohydr. Polym.*, 2018, **190**(2018), 148–155, DOI: 10.1016/j.carbpol.2018.02.019.

18 F. Hajiali and J. Vidal, Extraction of Chitin from Green Crab Shells by Mechanochemistry and Aging, *ACS Sustainable Chem. Eng.*, 2022, **10**(34), 11348–11357, DOI: 10.1021/acssuschemeng.2c02966.

19 O. Nuri and K. Jeung Gon, Mechanochemical Post-Polymerization Modification: Solvent-Free Solid-State Synthesis of Functional Polymers, *ACS Macro Lett.*, 2018, **7**(5), 561–565, DOI: 10.1021/acsmacrolett.8b00171.

20 M. Manimohan and S. Pugalmani, Novel isatin–incorporated biopolymer Schiff base ligands extracted from lobster shell waste: synthesis, spectral characteristics, and promising metal ion up-taking property, *Biomass Convers. Biorefin.*, 2024, **14**, 32241–32257, DOI: 10.1007/s13399-023-04872-9.

21 M. Manimohan and M. Rahaman, Novel biomaterial comprising Schiff base extracted from Homarus americanus/Lobster shell waste: Biological activity and In-vitro anticancer efficacies, *Sustainable Chem. Pharm.*, 2023, **37**, 101363, DOI: 10.1016/j.scp.2023.101363.

22 M. A. Asrahwi, N. Aqilah Rosman, M. Ningsheh, *et al.*, Solid-state mechanochemical synthesis of chitosan from mud crab (Scylla serrata) chitin, *Carbohydr. Res.*, 2023, **534**, 108971, DOI: 10.1016/j.carres.2023.108971.

23 A. B. Muley and M. R. Ladole, Intensification in biological properties of chitosan after γ-irradiation, *Int. J. Biol. Macromol.*, 2019, **131**, 435–444, DOI: 10.1016/j.ijbiomac.2019.03.072.

24 Z. Fan and Y. Qin, Synthesis, characterization, and antifungal evaluation of diethoxyphosphoryl polyaminoethyl chitosan derivatives, *Carbohydr. Polym.*, 2018, **190**, 1–11, DOI: 10.1016/j.carbpol.2018.02.056.

25 S. Nadia and S. Mohammad, Preparation and characterization of porous chitosan-based membrane with enhanced copper ion adsorption performance, *React. Funct. Polym.*, 2020, **154**, 104681, DOI: 10.1016/j.reactfunctpolym.2020.104681.

26 V. M. Dinh and S. G. Khokarale, Ionic liquid strategy for chitosan production from chitin and molecular insights, *RSC Sustainability*, 2024, **2**, 1154–1164, DOI: 10.1039/D4SU00053F.

27 M. Murugaiyan and S. P. Mani, Zinc (ii) centered biologically active novel N, N, O donor tridentate water-soluble hydrazide-based O-carboxymethyl chitosan Schiff base metal complexes: synthesis and characterisation, *New J. Chem.*, 2019, **43**, 9540–9554, DOI: 10.1039/c9nj00670b.

28 M. Manimohan and R. Paulpandiyan, Biologically active Co (II), Cu (II), Zn (II) centered water soluble novel isoniazid grafted O-carboxymethyl chitosan Schiff base ligand metal complexes: Synthesis, spectral characterisation and DNA nuclease activity, *Int. J. Biol. Macromol.*, 2020, **163**, 801–816, DOI: 10.1016/j.ijbiomac.2020.06.278.

29 R. Malav and S. Ray, Recent advances in the synthesis and versatile applications of transition metal complexes featuring Schiff base ligands, *RSC Adv.*, 2025, **15**, 22889–22914, DOI: 10.1039/D5RA03626G.

30 M. Manimohan and S. Pugalmani, Synthesis, spectral characterisation and biological activities of novel biomaterial/N, N, O donor tridentate Co (II), Ni (II) and Zn (II) complexes of hydrazide based biopolymer Schiff base ligand, *J. Inorg. Organomet. Polym. Mater.*, 2020, **30**, 4481–4495, DOI: 10.1007/s10904-020-01578-7.

31 M. Manimohan and S. Pugalmani, Biologically active novels N, N, O donor tridentate water soluble hydrazide based O-carboxymethyl chitosan Schiff base Cu (II) metal complexes: Synthesis and characterisation, *Int. J. Biol. Macromol.*, 2019, **136**, 738–754, DOI: 10.1016/j.ijbiomac.2019.06.115.

32 M. M. El-Zahed and M. A. Diab, Antibacterial, antifungal, DNA interactions, and antioxidant evaluation of Cu(II) Co(II), Ni(II), Mn(II) and UO2(II) mixed ligand metal complexes: Synthesis, characterization and molecular docking studies, *Mater. Sci. Eng., B*, 2024, **299**, 116998, DOI: 10.1016/j.mseb.2023.116998.

33 S. A. Jasim and Y. Riadi, Nanomagnetic macrocyclic Schiff-base–Mn(II) complex: an efficient heterogeneous catalyst for click approach synthesis of novel β-substituted 1,2,3-triazoles, *RSC Adv.*, 2022, **12**, 17905–17918, DOI: 10.1039/D2RA02587F.

34 K. Ahmed, G. Saikia, P. Begum, *et al.*, Selective and Green Sulfoxidation in Water using a New Chitosan Supported Mo(VI) Complex as Heterogeneous Catalyst, *ChemistrySelect*, 2018, **3**, 12563–12575, DOI: 10.1002/slct.201803000.

35 R. Franich, A. Singh, S. Gallagher, *et al.*, Comment on the structure of osmium tetroxide-chitosan complex, *Comments Inorg. Chem.*, 2011, **32**(1), 39–52, DOI: 10.1080/02603594.2011.593212.

36 R. Gup and C. Gokce, Seven-coordinated cobalt (II) complexes with 2,6-diacetylpyridine bis(4-hydroxybenzoylhydrazone): synthesis, characterisation, DNA binding and cleavage properties, *Supramol*, 2015, **27**(10), 629–641, DOI: 10.1080/10610278.2015.1051978.

37 C. Gokce, Synthesis, Crystal Structure and In Vitro Cytotoxicity of Novel Cu (II) Complexes Derived from Isatin Hydrazide-Hydrazone Ligands, *Acta Chim. Slov.*, 2023, **70**, 620–627, DOI: 10.17344/acsi.2023.8398.

38 S. Yadav and I. Yousuf, Synthesis and spectroscopic characterization of diorganotin (iv) complexes of N′-(4-hydroxypent-3-en-2-ylidene) isonicotinohydrazide: chemotherapeutic potential validation by in vitro interaction studies with DNA/HSA, DFT, molecular docking and cytotoxic activity, *RSC Adv.*, 2015, **5**(63), 50673–50690, DOI: 10.1039/c5ra06953j.

39 N. G. Alexey and A. K. Mikhail, Schiff Base Zinc (II) Complexes as Promising Emitters for Blue Organic Light-

Emitting Diodes, *ACS Appl. Electron. Mater.*, 2021, **3**, 3436–3444, DOI: 10.1021/acsaelm.1c00402.

40 Y. Lin and Z. Meihong, A general strategy to synthesis chitosan oligosaccharide-O-Terpenol derivatives with antibacterial properties, *Carbohydr. Res.*, 2021, **503**, 108315, DOI: 10.1016/j.carres.2021.108315.

41 Y. Zhang and X. Li, A novel zinc complex with antibacterial and antioxidant activity, *BMC Chem.*, 2021, **15**, 17, DOI: 10.1186/s13065-021-00745-2.

42 L. Zhenhao, B. Shicheng, D. Guangwu, *et al.*, Self-Reinforced and Antibacterial Zn2+ @Vanillin/Carboxymethyl Chitosan Film for Food Packaging, *ACS Sustain. Chem. Eng.*, 2023, **11**(34), 12747–12758, DOI: 10.1021/acssuschemeng.3c03109.

43 M. Arif Ali, U. Anjali, M. Apurba, *et al*, Visible-Light-Responsive Novel Ru(II)-Metallo-Antibiotics with Potential Antibiofilm and Antibacterial Activity, *ACS Appl. Mater. Interfaces*, 2024, **16**(22), 28118–28133, DOI: 10.1021/acsami.4c02979.

44 N. Mammari, E. Lamouroux, A. Boudier, *et al*, Current Knowledge on the Oxidative-Stress-Mediated Antimicrobial Properties of Metal-Based Nanoparticles, *Microorganisms*, 2022, **10**(2), 437, DOI: 10.3390/microorganisms10020437.

45 S. Thangudu and C. H. Su, Review of light activated antibacterial nanomaterials in the second biological window, *J. Nanobiotechnol.*, 2025, **23**, 293, DOI: 10.1186/s12951-025-03333-x.

46 E. Ren, C. Zhang, D. Li, *et al*, Leveraging metal oxide nanoparticles for bacteria tracing and eradicating, *View*, 2020, **1**(3), 20200052, DOI: 10.1002/VIW.20200052.

47 J. Zhou and Y. Cai, Breaking down the cell wall: Still an attractive antibacterial strategy, *Front. Microbiol.*, 2022, **13**, 952633, DOI: 10.3389/fmicb.2022.952633.

48 Q. Li and W. Tan, Novel triazolyl-functionalized chitosan derivatives with different chain length of aliphatic alcohol substituent: design, synthesis, and antifungal activity, *Carbohydr. Res.*, 2015, **418**, 44–49, DOI: 10.1016/j.carres.2015.10.005.

49 L. Wei and Y. Mi, Evaluation of quaternary ammonium chitosan derivatives differing in the length of alkyl side-chain: Synthesis and antifungal activity, *Int. J. Biol. Macromol.*, 2018, **129**, 1127–1132, DOI: 10.1016/j.ijbiomac.2018.09.099.